Networked Nanoparticle Arrays for Autonomous Computing

(Invited Paper)

Xingfei Wei[†], Ewa Harazinska[†], Yinong Zhao[‡] and Rigoberto Hernandez[*†‡§]
[†]*Department of Chemistry*, *Johns Hopkins University*, Baltimore, Maryland 21218, USA
[‡]*Department of Chemical & Biomolecular Engineering*, *Johns Hopkins University*, Baltimore, Maryland 21218, USA
[§]*Department of Material Science & Engineering*, *Johns Hopkins University*, Baltimore, Maryland 21218, USA
[*]Corresponding author, Email: r.hernandez@jhu.edu

***Abstract*—We have pursued the use of polymer-networked engineered nanoparticles as a candidate material capable of retaining information or perhaps even processing information in some prescribed way. Such operations would be of use for the neuromorphic engineering of materials that can compute intrinsically—that is, that they are in no way subject to a von Neumann architecture—and they have been identified as autonomous computing materials. Using trajectories integrated to much longer time steps than previously observed, we can now confirm that the response of the polymer-networked engineered nanoparticle arrays are highly sensitive to external perturbations. That is, the specific internal connections around given nanoparticles can be assigned to states useful for information processing, and the variations in their physical properties can result in specific responses allowing the state to be read. Moreover, their resulting equilibrium properties also depend on such external driving, and hence are subject to control which is a minimal requirement for these materials to be candidates for autonomous computing. We also demonstrate that using long polymer chains can help regulate the networks structures by increasing the 1st nearest links and reducing other links.**

***Index Terms*—engineered nanoparticles, materials design, coarse-grained dynamics, computing primitives**

I. Introduction

Over the last decade, it has become clear that conventional very-large-scale integration (VLSI) is reaching key scaling limits [1], [2], [3], [4]. Meanwhile, the energy efficiency of human-engineered electronic devices is many orders of magnitude lower as compared to biological computational structures. The pursuit of devices that are capable of mimicking brain function often emphasizing the processing of spike trains, has led to the many successes in the field of neuromorphic engineering [5], [6], [7]. The discovery of memristors [8], [9] completed the scope of possible basic electronic components that can relate voltage, charge current, and flux bilinearly to each other. It has been critical to the design of modern-day neuromorphic chips [10], [11], [12], [9], [13], [14]. However, this line of research has mostly remained tied to the use of semiconductor components that are invariably limited by the lengths that cannot be smaller than the width spanned by a few silicon atoms.

We therefore need a new class of materials that can enable computing but which are not bound by the rules of conventional VLSI, and we are inspired by the fact that the brain is an existence proof for such low-energy consumption and high-computing speed materials that do not rely on a von Neumann architecture [15], [16], as it operates at exascale speeds while consuming about 20 W energy [17]. In our recent papers [18], [19], we demonstrated that two and three dimensional arrays of polymer connected gold nanoparticles (AuNPs) could exhibit emergent structure in response to external fields, and posited that these arrays could be used as autonomous computing materials (ACMs) [16]. In these 2D engineered nanoparticle (ENP) array, connections are formed primarily by Coulombic forces, which makes the network structure reprogrammable and volatile. In the current work, we show the network dynamics of the 2D square (SQ) ENP array at long-enough simulation times. This conclusion is accessible here because we report coarse-grained (dissipative particle dynamics (DPD)) simulations integrated to a much longer time—viz 400 million steps—than previously reported—viz 60 million steps—by nearly an order of magnitude. The network structures can be mapped onto different physical properties and data states, which is necessary for processing information. We also demonstrate how the network connectivity and other emergent properties are affected by the nature and number of polymers linking the AuNPs.

II. Simulation Model

A. 2D SQ ENP array

The details of the DPD simulation model construction can be found in our previous work [18], [19]. In brief, each ENP has a 4 nm diameter AuNP core and a polymer poly(allylamine hydrochloride) (PAH) with 200 repeating units. The coarse-grained (CG) AuNP model assumes 400 Au atoms at the surface, and CG PAH uses 2 particles to represent each repeating unit. We set the charge of 200 Au atoms—selected uniformly—to -1 e to represent the citrate capped AuNP (cit-AuNP) on the surface[20], [21], [22], [23]. Each PAH chain with 200 repeating units is fully ionized and each

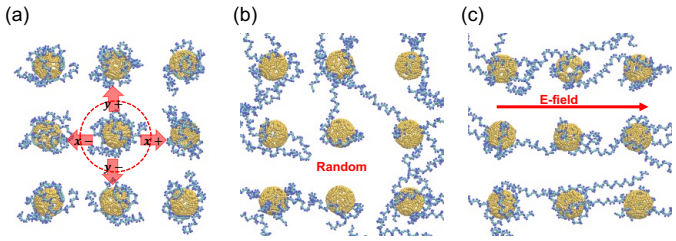

Fig. 1. ENP in 2D SQ regular array with a distance of 10 nm between two ENPs. (a) The four 1st nearest links in $x+$, $x-$, $y+$, and $y-$ directions. (b) Scheme of an isotropic network by temperature activation. (c) Scheme of an anisotropic network by E-field regulation.

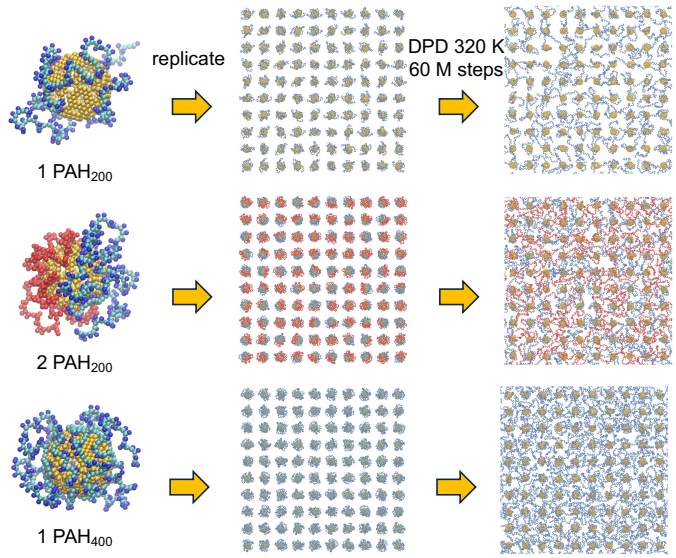

Fig. 2. Simulation models with differing PAH chain compositions and structure: single PAH_{200}, double PAH_{200}, and single PAH_{400} on each ENP.

repeating unit carries +1 e charge. As a result, the overall charge for each ENP is neutral. A 10×10 ENP regular array of these particles is constructed by replicating with random rotations of an ENP at the vertices of a 2D square lattice with a 10 nm lattice constant; see Figs. 1 and 2. Random rotations of the polymers around the nanoparticles provide nontrivial new network structures due to their asymmetry. In the current model, the PAHs are not electrically conductive, but the network structure of PAH-AuNP can regulate ion transport and ionic conductivity to access different states.

B. Simulation protocol

The initial structure has no network connections between ENPs; see Fig. 1a. The ENP-polymer binding interaction results from Lennard-Jones (LJ) and Coulombic forces, the polymer-polymer interaction is modeled using a DPD force, and the E-field-polymer interaction is driven by the electrostatic force [18], [19]. Each PAH chain can make a move and build connections in 4 different directions—viz. $x+$, $x-$, $y+$, and $y-$. With increasing temperature, PAHs are increasingly likely to be activated by random forces and can generate isotropic network structures; see Fig. 1b. When applying an E-field, PAHs are driven by the E-field direction and generate anisotropic networks; see Fig. 1c. In recent work [18], [19], we have already performed parametric studies on the network connections, at various E-field strengths and temperatures. We use the Large-scale Atomic Molecular Massively Parallel Simulator (LAMMPS) package to propagate all simulations [24]. Our simulation time step size is 1 CG DPD time, which represents > 1 fs for each step [18], [19]. A typical production simulation time is 60 million steps [18], [19]. For temperature activated models, the network connection simulations can approach equilibrium. However, for the E-field driven models, the network connection simulations are far from equilibrium. To improve the network dynamics simulation, we extend the simulation time to 200 to 400 million steps and calculate the number of links in different directions.

C. Change PAH number and chain length

We have designed new AuNP models using 2 PAH_{200} chains and 1 PAH_{400} chain to compare with the 1 PAH_{200} chain model on the 2D SQ array; see Fig. 2. For 2 PAH and 1 PAH_{400} models, the AuNP core is set with -1 e/atom and a total of -400 e to neutralize the PAHs. We run 60 million steps to simulate the network connections in these 3 models at temperatures from 60 K to 500 K; see Fig. 2 for representative schemes of network connections at 320 K. The degree of valency of the AuNPs affects the resulting network structure [25]. In the present case, AuNPs have a valency of 2 because of polymer-polymer exclusion effects and the limited area available on a given AuNP surface. The sum of all first nearest links ($\sum n_i$) and the number of other links (n_{other}) are reported. Since the network structure is isotropic using temperature activation, we expect the n_{x+}, n_{x-}, n_{y+}, and n_{y-} values to be similar.

III. Results and Discussion

Constrained by the available computing time, we previously reported the behavior of the network connections in prototype ACMs—viz SQ arrays—for times corresponding to 40 to 60 million DPD simulation steps [18], [19]. This was reasonable because the underlying atomistic simulation models are also carried out at the nanosecond time scales. However, much longer simulation times are required to characterize the dynamics of some of the polymer network structures reported here. Consequently, theDPD simulations were run for times up to 200 to 400 million steps for the 2D SQ array under three different conditions—viz. no E-field 320 K, $E_x = 0.000112$ V/Å ($E_x = 10h$) 160 K, and $E_x = 0.0000112$ V/Å ($E_x = 1h$) 320 K; see Fig. 3.

A. Temperature Activated Isotropic Network

Increasing temperature to 320 K can activate a PAH even though the driving force on the polymer chain is random. It generates structures that appear as the random walks seen in polymer diffusion. Under no applied e-field, we found a small peak at 200 million simulation steps in the net orientation

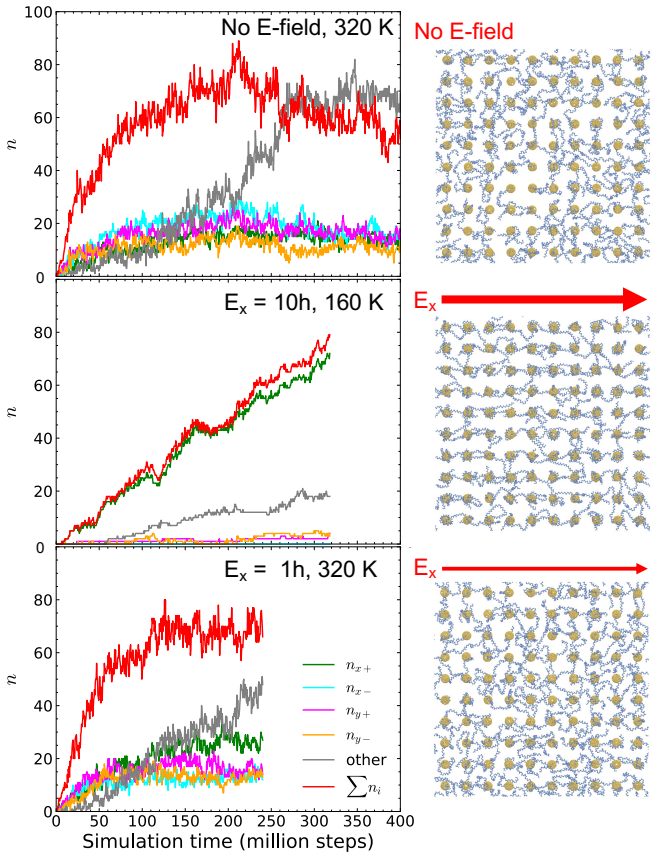

Fig. 3. Long time dynamics and stability of network structures. The top panel shows isotropic link connections for 400 million simulation steps, at scaled temperature equal to 320 K. The middle panel shows anisotropic link connections for 315 million simulation steps, at scaled temperature equal to 160 K. The bottom panel shows slightly anisotropic link connections for 240 million simulation steps, at scale temperature 320 K. Representative schemes of final frames are given on the right side. All panels share the same legend shown in the bottom panel: 1st nearest links in $x+$, $x-$, $y+$, and $y-$ are labeled as n_{x+}, n_{x-}, n_{y+}, and n_{y-}, respectively. $\sum n_i$ is the sum of n_{x+}, n_{x-}, n_{y+}, and n_{y-}. n_{other} represents other links not belonging to n_i. The scaled E-field magnitude $h = 0.0000112$ V/Å.

(or connectivity) $\sum n_i$, but this transient net orientation is fleeting, and it appears that such systems equilibrate (with nearly zero net orientation) at 60 million simulation steps; see the top panel in Fig. 3. Meanwhile, we found that n_{other} increases significantly with time in our DPD simulations until nearly 250 million simulation steps, when it finally reaches an equilibrium. Thus at shorter times, the polymer chains reach the nearest ENPs, making links primarily between 1st nearest neighbor AuNPs. We thus found that simulation times up to 60 million steps tend to be enough to recover network structures when the 1st nearest links dominate. In such cases, we found earlier that a Spin-Ising Potts model, whether solved by mean field theory (MFT) approximation or Monte Carlo (MC) simulation, provided good agreement in the observed link structures temporally and at equilibrium [18], [19]. On the other hand, when the polymers begin to link ENPs beyond nearest neighbors, characteristic relaxation and equilibrium required simulations with more than 250 million simulation steps which lies within the regime reported here.

B. E-field Regulated Anisotropic Networks

Applying an E-field can drive positively charged PAH chains to align with the E-field direction. This field can be used to regulate ionic conductivity inside ENP arrays because ions move faster along the polymer alignment direction, but they are jammed in the orthogonal direction. When the E-field is strong, at $\text{E}_x = 10h$ ($\text{E}_x = 0.000112$ V/Å) 160 K, the links in the positive ($x+$) direction n_{x+} dominate the total sum, $\sum n_i$; see the middle panel in Fig. 3. For this strong-driving regime, we find that n_{x+} continues to increase linearly even at the last DPD simulation step of 315 million steps reported here. Meanwhile, n_{other} seems to approach equilibrium after 200 million steps, likely due to the relatively low temperature of the system. For comparison, we also performed simulations under a reduced E-field strength at $E_x = 1h$ ($E_x = 0.0000112$ V/Å), and an increased temperature at 320K; see the bottom panel in Fig. 3. We then find that both $\sum n_i$ and n_{x+} appear to reach equilibrium starting at 120 million steps, but n_{other} continues to increase even at 240 million steps; see the bottom panel of Fig. 3. We also find that n_{x+} is slightly larger than n_{x-}, n_{y+} or n_{y-}, because the E-field driving force is comparable to the temperature driving random force. Our simulations thus demonstrate that by tuning the E-field, system temperature, and simulation time, we can create predictable and varied network structures on the ENP array. Using a top-down MC model, whose parameters are found from bottom-up molecular dynamics (MD) simulations, [18], [19] much longer simulation time and length scales can be accessed for these systems under E-Field. In turn, the MC model was used to confirm that those MD simulations posited above to reach near their equilibrium limits did so.

C. Network connections in the 2 PAH$_{200}$ model

Although longer-time simulations are sometimes required (and reported in this work), for many of our simulations, we integrate only up 60 million steps. Such "shorter" runs require 1-2 weeks of system computer time to complete on our HPC resources, which is already computationally expensive, and they are enough to offer direct comparison with our previous work [18], [19]. As we reported in section III-A above, this simulation time is just enough to allow the 1st nearest links to reach equilibrium for temperature activated random networks. The top panels in Fig. 4 show the network connections, $\sum n_i$ and n_{other}, for the 1 PAH$_{200}$ model. When each ENP has 2 PAH$_{200}$ chains in the 2 PAH$_{200}$ model, the number of 1st nearest links and other links are larger than those for the 1 PAH$_{200}$ model; see the middle panels in Fig. 4. As should be expected, when more polymers are available to bind between ENPs, the ENPs are consequently more strongly linked; see the middle schemes in Fig. 3. For example, at 320 K the $\sum n_i$ increases by 30% in the 2 PAH$_{200}$ model. However, such differences begin to appear only when the system temperature is at least 300-500 K; see Fig. 5. This is because the network

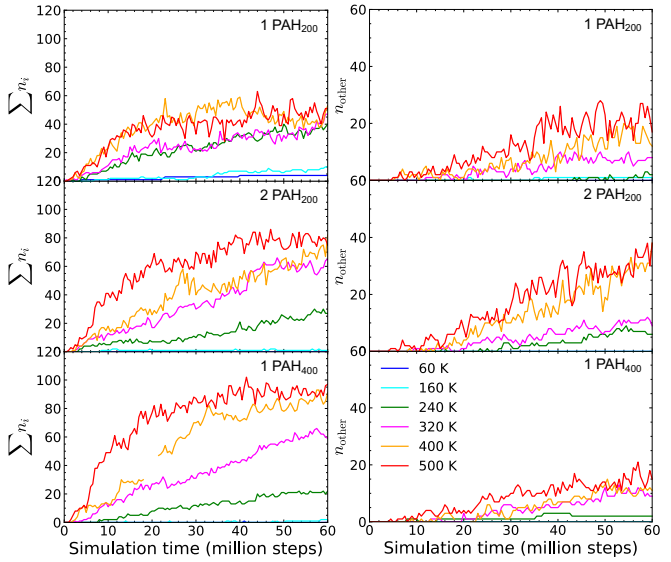

Fig. 4. Comparison of the network connections for 3 different ENP cases with 60 million steps. From top to bottom, each ENP has 1 PAH_{200}, 2 PAH_{200}, and 1 PAH_{400}, respectively. The left panels show 1st nearest links $\sum n_i$ at different temperatures. The right panels show other links $n_{\rm other}$ at different temperatures. All panels share the same legend shown in the bottom right panel.

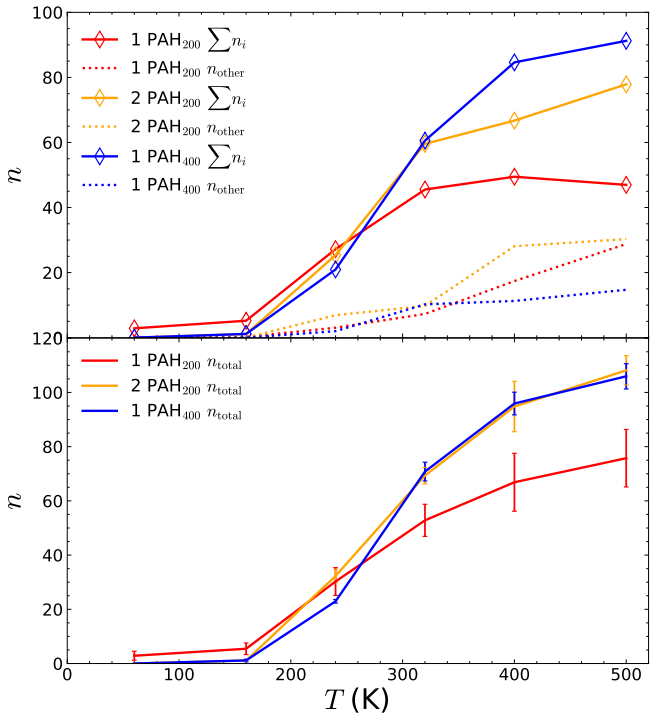

Fig. 5. Comparison of the averaged number of links for ENP models with 1 PAH_{200}, 2 PAH_{200}, and 1 PAH_{400}: 1st nearest links $\sum n_i$ and other links $n_{\rm other}$ (top panel), and total number of links ($n_{\rm total}$=$\sum n_i$+$n_{\rm other}$) (bottom panel). The average link numbers are calculated from 50 to 60 million steps.

dynamics are fast enough at higher temperatures to form and equilibrate the structure. At lower temperatures, $T < 300$ K, it takes longer for the polymer to form even the first link between the ENPs, and the presence of two possible such binders does not speed it up enough to structure the network.

D. Comparison between PAH_{200} and PAH_{400} models

We now double the polymer chain length to make the total number of PAH units on a single ENP—viz PAH_{400} model—the same as that of a model system with two chains of PAH_{200}. Schemes of the single PAH_{400} model are shown in the bottom panel of Fig. 3. As the single PAH_{400} and double PAH_{200} models contain the same number of monomers, comparison of their resulting dynamics reveals the sensitivity of the system to the nature of their connectivity. First, perhaps unsurprisingly, we found more 1st nearest links in the single PAH_{400} model than in the double PAH_{200} model, especially at high temperatures, as shown in Fig. 5 top panel. Second, we found the fewest number of other links in the single PAH_{400} model, when comparing between both single PAH_{400} and double PAH_{200} models; see Fig. 4. Interestingly, the total number of links $\sum n_i$—viz, the sum of links not in $n_{\rm other}$—are similar in the temperature activated random networks at 300-500 K resulting from both the double PAH_{200} and single PAH_{400} models; see Fig. 5 bottom panel. At lower temperatures, we need to use longer simulation time to find the resulting equilibrium network structures. Relative to multiple short chain polymers, using a single long-chain polymer can confine the polymer and reduce the random diffusion distance. This tends to reduce the formation of other links by avoiding its binding to distant ENPs, which can thereby increase the probability of creating 1st nearest links.

IV. Conclusions

In this work, we extended our DPD simulation times to demonstrate that for temperature driven random networks, the 1st nearest links can approach an equilibrium in about 60 million steps, but the other links need more than 250 million steps to reach equilibrium. The ENP array in this model is effectively a single device of ~ 100 nm in width, which can adopt one of many states through control of electric field and temperature. It thereby allows for sequential processing of information when subjected to a time series of varying external perturbations. For E-field regulated anisotropic network connections, the E-field strength and system temperature are both important to the dynamics of the network structure. At low temperatures with strong E-field, all of the links are driven by the E-field, and the resulting 1st nearest links are aligned with the E-field. At high temperatures with weak E-field, most of the links are driven by the random force, and the resulting network connection is slightly anisotropic with a large number of other links.

We also find that using either two polymers—viz two PAH_{200}—or using one longer polymer—viz one PAH_{400}—can increase the number of 1st nearest links, relative to that from a single PAH_{200} model. The total number of links are the same for both double PAH_{200} and single PAH_{400} models. The number of other links in the double PAH_{200} model is much

larger than that in the single PAH_{400} model. We also find that the single PAH_{400} model has significantly more 1st nearest links than the double PAH_{200} model. This advantage for long chain polymers can serve as a lever for guiding the design of ENP-polymer network structures in various engineering applications. For example, by programming and training the network structure, we conjecture the possibility of regulating ionic conductivity so as to construct and maintain states useful in storing and preserving data.

ACKNOWLEDGMENTS

This work has been partially supported by the National Science Foundation (NSF) through Grant No. CHE 2102455. The computing resources necessary for this work were performed in part on Expanse at the San Diego Supercomputing Center through allocation CTS090079 provided by Advanced Cyberinfrastructure Coordination Ecosystem: Services & Support (ACCESS), which is supported by National Science Foundation (NSF) grants #2138259, #2138286, #2138307, #2137603, and #2138296. Additional computing resources were provided by the Advanced Research Computing at Hopkins (ARCH) high-performance computing (HPC) facilities.

REFERENCES

[1] R. S. Williams, "What's next? [the end of moore's law]," *Comput. Sci. Eng.*, vol. 19, no. 2, pp. 7–13, 2017.

[2] T. N. Theis and H.-S. P. Wong, "The end of moore's law: A new beginning for information technology," *Comput. Sci. Eng.*, vol. 19, no. 2, pp. 41–50, 2017.

[3] J. Shalf, "The future of computing beyond moore's law," *Philos. Trans. R. Soc., A*, vol. 378, no. 2166, p. 20190061, 2020.

[4] C. Walter, "Kryder's law," *Sci. Am.*, vol. 293, pp. 32–33, 2005.

[5] C. Mead, "Neuromorphic electronic systems," *Proceedings of the IEEE*, vol. 78, no. 10, pp. 1629–1636, 1990.

[6] ——, "How we created neuromorphic engineering," *Nat. Electron.*, vol. 3, pp. 434–435, 2020.

[7] J. Zhu, T. Zhang, Y. Yang, and R. Huang, "A comprehensive review on emerging artificial neuromorphic devices," *Appl. Phys. Rev.*, vol. 7, no. 1, p. 011312, 2020.

[8] D. B. Strukov, G. S. Snider, D. R. Stewart, and R. S. Williams, "The missing memristor found," *Nature (London)*, vol. 453, p. 80–83, 2008.

[9] Y. Zhang, Z. Wang, J. Zhu, Y. Yang, M. Rao, W. Song, Y. Zhuo, X. Zhang, M. Cui, L. Shen, R. Huang, and J. J. Yang, "Brain-inspired computing with memristors: Challenges in devices, circuits, and systems," *Appl. Phys. Rev.*, vol. 7, no. 1, p. 011308, 2020.

[10] T. Serrano-Gotarredona, T. Masquelier, T. Prodromakis, G. Indiveri, and B. Linares-Barranco, "Stdp and stdp variations with memristors for spiking neuromorphic learning systems," *Front. Neurosci.*, vol. 7, p. 2, 2013.

[11] S. Furber, "Large-scale neuromorphic computing systems," *J. Neural Eng.*, vol. 13, 2016.

[12] H. Ling, D. A. Koutsouras, S. Kazemzadeh, Y. van de Burgt, F. Yan, and P. Gkoupidenis, "Electrolyte-gated transistors for synaptic electronics, neuromorphic computing, and adaptable biointerfacing," *Appl. Phys. Rev.*, vol. 7, no. 1, p. 011307, 2020.

[13] Y. Tuchman, T. N. Mangoma, P. Gkoupidenis, Y. V. D. Burgt, R. A. John, N. Mathews, S. E. Shaheen, R. Daly, G. G. Malliaras, and A. Salleo, "Organic neuromorphic devices: Past, present, and future challenges," *MRS Bulletin*, vol. 45, no. 8, pp. 619–630, 2020.

[14] S. Bains, "The business of building brains," *Nat. Electron.*, vol. 3, no. 7, pp. 348–351, 2020.

[15] V. K. Sangwan and M. C. Hersam, "Neuromorphic nanoelectronic materials," *Nat. Nanotechnol.*, vol. 15, pp. 517–528, 2020.

[16] M. Bathe, R. Hernandez, T. Komiyama, R. Machiraju, and S. Neogi, "Autonomous computing materials," *ACS Nano*, vol. 15, no. 3, p. 3586–3592, 2021.

[17] N. R. B. Martins, A. Angelica, K. Chakravarthy, Y. Svidinenko, F. J. Boehm, I. Opris, M. A. Lebedev, M. Swan, S. A. Garan, J. V. Rosenfeld, T. Hogg, and R. A. Freitas Jr, "Human brain/cloud interface," *Front. Neurosci.*, vol. 13, p. 112, 2019.

[18] X. Wei, Y. Zhao, Y. Zhuang, and R. Hernandez, "Engineered nanoparticle network models for autonomous computing," *J. Chem. Phys.*, vol. 154, p. 214702, 2021.

[19] X. Wei, E. Harazinska, and R. Hernandez, "Control of structure and dynamics in polymer-networked engineered nanoparticle arrays by electric fields," *Phys. Rev. Res.*, vol. 5, p. L022057, 2023.

[20] G. Chong and R. Hernandez, "Adsorption dynamics and structure of polycations on citrate-coated gold nanoparticles," *J. Phys. Chem. C*, vol. 122, p. 19962–19969, 2018.

[21] G. Chong, E. D. Laudadio, M. Wu, C. J. Murphy, R. J. Hamers, and R. Hernandez, "Density, structure, and stability of $\mathrm{citrate}^{3-}$ and $\mathrm{H_2citrate}^{-}$ on bare and coated gold nanoparticles," *J. Phys. Chem. C*, vol. 122, pp. 28 393–28 404, 2018.

[22] X. Wei, Y. Zhao, Y. Zhuang, and R. Hernandez, "Building blocks for autonomous computing materials: Dimers, trimers and tetramers,," *J. Chem. Phys.*, vol. 155, p. 154704, 2021.

[23] X. Wei, A. Popov, and R. Hernandez, "Electric potential of citrate capped gold nanoparticles is affected by poly(allylamine hydrochloride) and salt concentration," *ACS Appl. Mater. Interfaces*, vol. 14, p. 12538–12550, 2022.

[24] S. J. Plimpton, "Fast parallel algorithms for short-range molecular dynamics," *J. Comput. Phys.*, vol. 117, no. 1, pp. 1–19, 1995.

[25] X. Wei, C. Chen, Y. Zhao, E. Harazinska, M. Bathe, and R. Hernandez, "Molecular structure of single-stranded DNA on the ZnS surface of quantum dots," *ACS Nano*, vol. 16, p. 6666–6675, 2022.